# We are IntechOpen,
## the world's leading publisher of Open Access books
## Built by scientists, for scientists

**6,900**
Open access books available

**185,000**
International authors and editors

**200M**
Downloads

**154**
Countries delivered to

Our authors are among the

**TOP 1%**
most cited scientists

**12.2%**
Contributors from top 500 universities

**CLARIVATE ANALYTICS**
**BOOK CITATION INDEX**
**INDEXED**

**WEB OF SCIENCE™**

Selection of our books indexed in the Book Citation Index
in Web of Science™ Core Collection (BKCI)

## Interested in publishing with us?
## Contact book.department@intechopen.com

# Surface Modification of Mg Alloys AZ31 and ZK60-1Y by High Current Pulsed Electron Beam

Gao Bo, Hao Yi, Zhang Wenfeng and Tu Ganfeng
*School of materials and metallurgy, Northeastern University, Shenyang*
*China*

## 1. Introduction

The quality of Mg alloys with high specific modulus and specific strength is the lightest in the structural materials. Their density is about 2/3 of aluminium alloys and 1/4 of steels. The weight of whole structural materials is decreased drastically owing to some components or parts produced by Mg alloys. Thus, Mg alloys are widely used in aerospace, weapons, automobile and other fields [1-3]. Meanwhile, Mg alloys has many other advantages, such as excellent electromagnetic shielding performance, shock absorption ability, electric and heat conductivity, etc [4-6]. However, the chemical stability of Mg is very low, and its electrode potential is negative (-2.34V). As a result, the corrosion resistance of Mg alloys is poor in acid and neutral mediums. Furthermore, other properties of Mg alloys, wear resistance, hardness and resistance to high temperature, are also poor. Consequently, the superiority of Mg alloys in the application is restricted to some extent. Nowadays, the researches are concentrated on the improvement of hardness, wear and corrosion resistance of Mg alloys. Energy beam surface modification is an important developing direction, such as plasma micro-arc oxidation [7-11], laser surface treatment [12-16], ion beam surface modification [17-19], etc.

A.V. Apelfeld et al [10] have studied oxide protective coatings on the surface of Mg alloys obtained by micro-arc oxidation (MAO). A model of micro-arc coating formation is proposed. For Mg alloys, the structure of MAO coating plays an important role in improvement of corrosion resistance.

The research team (Y.M. Wang et al [11]) has investigated that dense oxide coatings formed in alkaline silicate electrolyte with and without titania sol addition are fabricated on AZ91D alloy using micro-arc oxidation. It reveals that the coating thickness decreases from 22μm to 18 μm with increasing concentration of titania sol from 0 to 10 vol. %. Electrochemical tests show that the Ecorr of Mg substrate positively shifts about 300-500 mV and Icorr lowers more than 100 times after micro-arc oxidation.

The literature [15] (A.K. Mondal et al) has reported that Mg alloy ACM720 is subjected to laser surface treatment using Nd:YAG laser in argon atmosphere. This treatment is beneficial for enhancing the corrosion and wear resistance of the alloy. The improved corrosion resistance is attributed to the absence of second phase $Al_2Ca$ at the rain boundaries, microstructural refinement and extended solid solubility, particularly of Al, in $\alpha(Mg)$ matrix owing to rapid solidification. The laser treatment also increases surface hardness two times and reduces the wear rate considerably due to grain refinement.

J. Dutta Majumdar and I. Manna [16] have researched that the mechanical properties of laser-surface-alloyed AZ91, a magnesium-based alloy (Mg-9Al-0.9Zn) with nickel. Laser surface alloying is carried out using a continuous wave $CO_2$ laser. As a result, laser surface alloying leads to the formation of a dispersion of intermetallics of Mg and Ni ($MgNi_2$) in an Mg matrix with an improved Young's modulus (45-85 GPa, as compared to the 45 GPa of as-received substrate) and improved wear resistance.

J.X. Yang et al [19] have found that thin carbon nitride (CN) coating can be deposited on Mg alloy substrate by ion beam assisted deposition. Through adjusting parameter, the coating with high N/C ratio of 0.38 is produced. The CN coating is a composition of amorphous $C_3N_4$ and improves the roughness of naked substrate from 32.9 nm to 28.9 nm. Moreover, the percentage increases of hardness and elastic modulus induced by coating are more than 90.6% and 82.8%, respectively.

Surface treatment of electron beam on metallic materials, such as steels, pure Al and Al alloys, NiTi alloy, has recently been investigated by domestic and foreign researchers [20-26]. It is found that metastable structures are formed on treated material surface and the hardness as well as wear and corrosion resistance is enhanced after electron beam treatment. However, the investigation on Mg alloys after electron beam treatment is reported rarely in literatures. In our group, the change in microstructure and properties of Mg alloys (AZ31, ZK60-1Y) has been researched in detail before and after HCPEB treatment.

## 2. Raw materials, devices and detection methods for experiment

### 2.1 Raw materials for experiment

The research objects of this passage are magnesium alloys AZ31 and ZK60-1Y. The chemical compositions of two Mg alloys refer to the table 2.1.

| Elements | Al | Zn | Zr | Y | Mn | Si | Cu | Fe | Ni | Mg |
|---|---|---|---|---|---|---|---|---|---|---|
| AZ31 | 2.5~3.5 | 0.6~1.4 | — | — | 0.2~1.0 | 0.1 | 0.05 | 0.005 | 0.005 | balance |
| ZK60-1Y | — | 6 | 0.5 | 1 | — | — | — | — | — | balance |

Table 2.1. Chemical compositions of Mg alloys AZ31and ZK60-1Y（*wt.%*）

### 2.2 The structure and technological parameters of the high current pulsed electron beam (HCPEB) device

The Fig. 2.1 refers to "Nadezhda-2" type HCPEB device [27] made in Russia. It consists of four parts, such as electron gun, vacuum system, power supply control system and diagnostic system. Vacuum system includes vacuum pump set (a set of molecular pump & a set of mechanical pump), vacuum chamber, vacuum valve as well as pipes for inputting cooling water and waste gas emission. Power supply control system includes high-voltage pulse generator and magnet field triggering power supply, etc. Diagnostic system includes relevant instruments and meters, such as operating vacuum measurement, electron beam, cathode accelerating voltage and average energy density, etc. Electron gun includes cathode, anode, spark source, rogowski coil and magnetic coil, etc. The electron gun used for generating high current pulsed electron beam is the core part of the whole equipment.
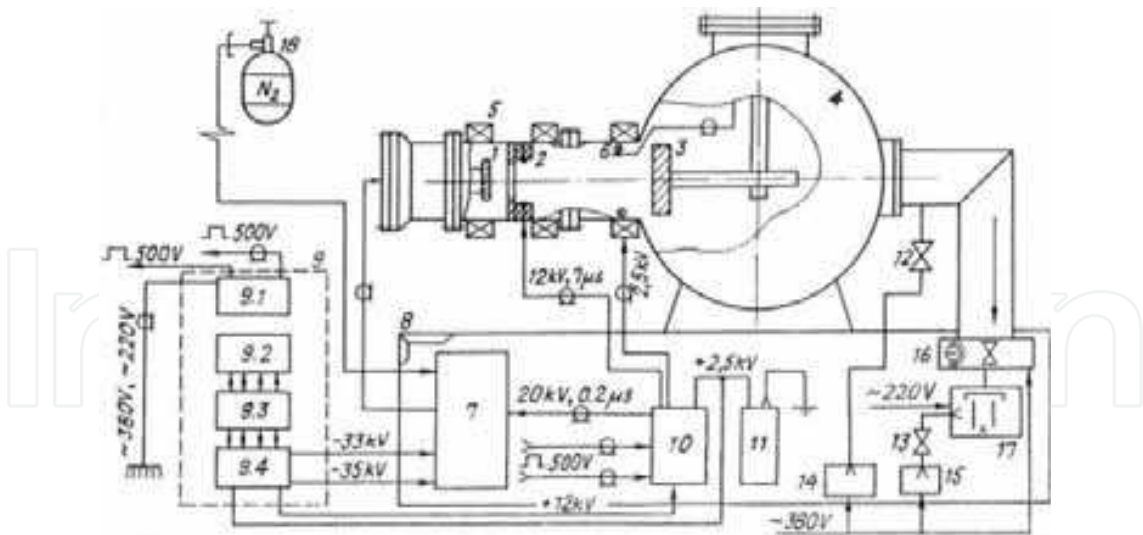
1-cathod; 2-spark source; 3-collector; 4-vacuum chamber; 5-solenoid; 6-rokovsky coil; 7-pulsed high-voltage generator; 8-bracket; 9-electricity controller; 10-pulses trigger; 11-capcitor; 12, 13-manual vacuum valve 1, 2; 14, 15-pump 1, 2; 16–electromagnetism valve, 17-molecular pump, 18-nitrogen.

Fig. 2.1. Schematic diagram of high current pulsed electron beam (HCPEB) system

"Nadezhda-2"type HCPEB device can generate a special form of electron beam. In this experiment, the main technological parameters are shown in table 2.2, in which the energy density of electron beam can be regulated through changing the capacitance of the high-voltage pulse generator, cathode accelerating voltage and adding magnetic field.

| Accelerating voltage /kV | Energy density /J/cm² | Pulse time /μs | Pulse frequency /Hz | Pulse number /Number | Target distance /mm | Beam spot diameter /mm |
|---|---|---|---|---|---|---|
| 27 | 3 | 1 | 0.1 | 5,10,15 | 140 | φ60 |

Table 2.2. Technological parameters for HCPEB equipment

## 2.3 Detection methods
### 2.3.1 Analysis of microstructure
The morphologies of surface and sectional microstructures of Mg alloys were analyzed through scanning electron microscope(SM-5600LV, SSX-550). Phase transformation of the treated surface of Mg alloys was conducted by using X-ray diffractometer (XRD-6000) with step size of $0.02^{o}$ and scanning range (2θ) of $20^{o}$~$100^{o}$. The experiment adopts a Cu Kα radiation source.

### 2.3.2 Friction and wear performance
The dry friction and wear tests of Mg alloy AZ31 surface were finished using a ball-on-flat apparatus at environmental temperature of 18~22℃. The sample surfaces were cleaned by acetone ultrasonic before friction and wear test. WC-Co balls with diameter 5mm were used as the sliding counterpart in all tests. The applied load was 5 N with a sliding velocity of 1 mm/s. The total sliding length and stroke length were 5mm and 1.2m, respectively.

Drying friction and wear testing of Mg alloy ZK60-1Y was conducted with a pin-on-disc type machine (MG-2000) at room temperature of 25℃. The samples used for experiment were cut into cylinders with diameter of Φ6mm and height of 12mm. The counterpart discs were made of stainless steel (1Cr18Ni9) with surface hardness of 192HV and surface roughness of 1μm ($R_a$). The applied load was 10N. The rotation speed was 250 r/min and the friction time was 10min.

### 2.3.3 Corrosion resistance

Polarization curves were performed in the EG&G M273 system. The experiment adopted three-electrode system. The reference electrode was saturated calomel electrode (SCE), the auxiliary electrode was Pt electrode, and the samples were working electrode. The test was performed in 5% NaCl solution and the corrosion testing surface area was 1cm$^2$.

## 3. Experiment results and discussion

### 3.1 Surface modification of Mg alloy AZ31 by HCPEB
### 3.1.1 Surface morphology

Fig. 3.1 gives the surface SEM morphologies of Mg alloy AZ31 after HCPEB treatment with energy density of 3J/cm$^2$. Fig. 3.1 (a) refers to the surface morphology of Mg alloy AZ31 after HCPEB treatment of 5 pulses. It can be apparently observed that a typical morphology emerges on the AZ31 Mg alloy surface after HCPEB treatment, namely wavy morphology after complete melting. With the pulse number increasing to 10 pulses, the "crater" morphology and few twins are found on the treated surface shown in the Fig. 3.1 (b). Fig. 3.1 (c) shows surface morphology of Mg alloy AZ31after 15 pulse treatment, it is found that the "crater" morphology disappears after repeated melting and a large number of twins are formed. The 15-pulsed sample surface tends to be smooth. The formation of twins is possibly induced by a lot of residual stresses on the surface after HCPEB treatment [28].
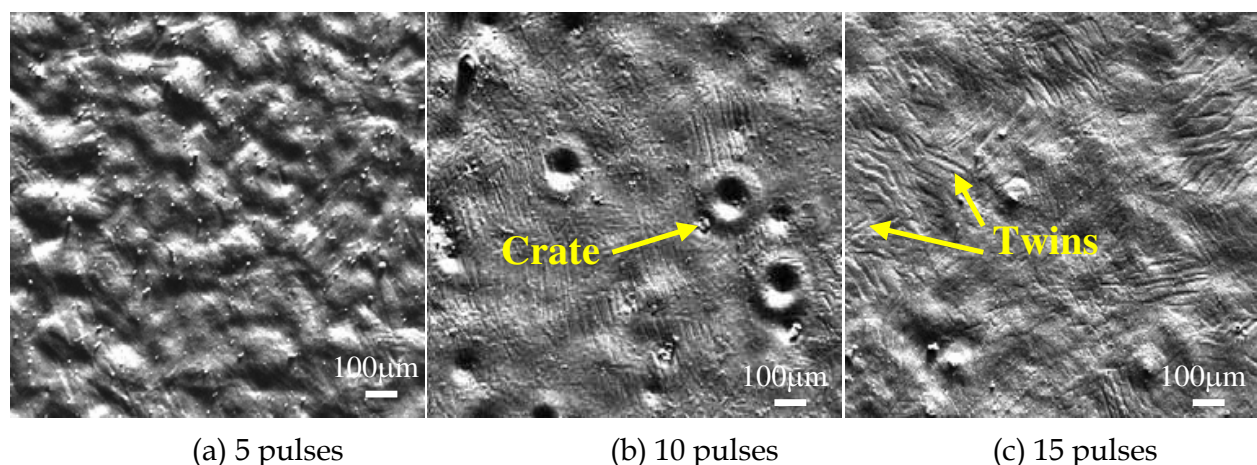


(a) 5 pulses                    (b) 10 pulses                    (c) 15 pulses

Fig. 3.1. Surface SEM morphologies of AZ31 Mg alloy after HCPEB irradiation with different pulses

### 3.1.2 Phase analysis

Fig. 3.2 indicates XRD patterns of Mg alloy AZ31 before and after HCPEB treatment and local analysis of (11-20) peaks. From the figure, it is found that the diffraction peaks of Mg

obviously move towards high-angle direction after 5 and 10 pulse treatments, as clearly shown in the enlarged figure. The moving of Mg diffraction peaks is more obvious with the increase of pulse number. This is generated by rapid heating and cooling process induced by HCPEB on the surface of Mg alloy. The substitutional solid solution of Al atoms replacing Mg atoms is formed in the Mg lattices, and the lattice constants are reduced as increasing solid solubility. To sum up, high-angle moving of Mg diffraction peaks is attributed to the formation of saturated solid solution of Mg [29].
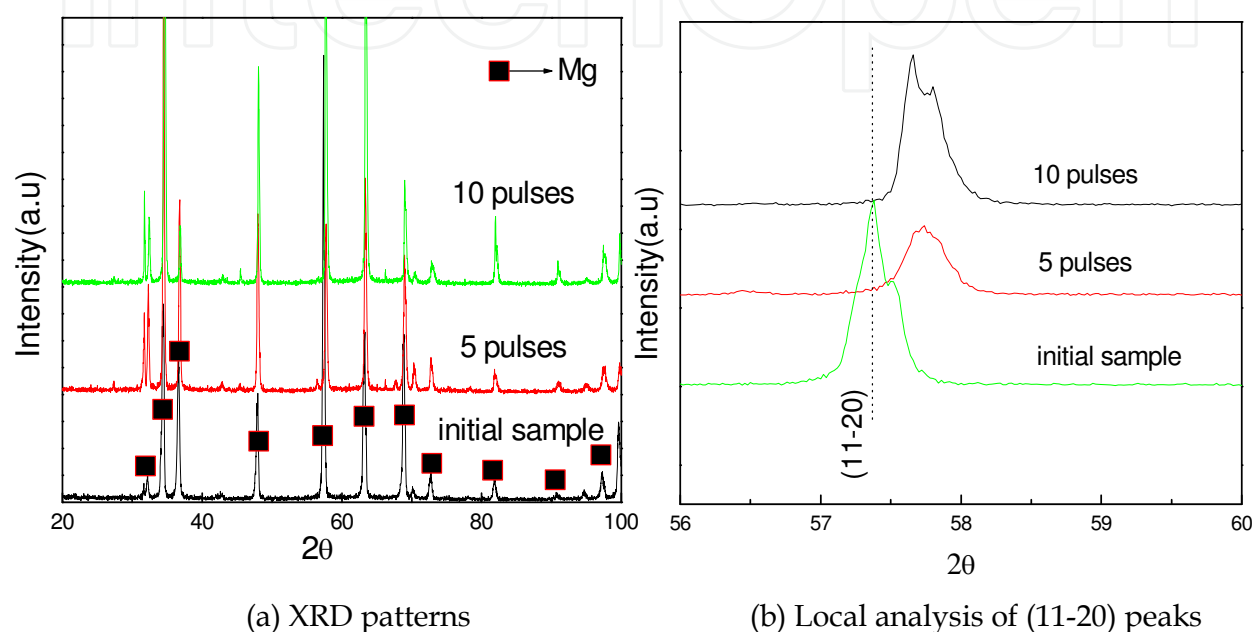


(a) XRD patterns                    (b) Local analysis of (11-20) peaks

Fig. 3.2. XRD patterns of Mg alloy AZ31before and after HCPEB treatment

### 3.1.3 Friction and wear property of Mg alloy AZ31

Fig. 3.3 indicates the evolution of friction coefficients with friction time and change of average friction rate with the number of pulses for Mg alloy AZ31 before and after HCPEB treatment. It can be seen that the friction coefficients of initial samples are only about 0.15 at the beginning (as seen in Fig.3.3(a)). It is due to a layer of hard MgO film on the surface. The oxide film is worn away after 5 minutes and the wear enters into severe wear stage, thus, the friction coefficients suddenly rise to 0.32~0.37. But the friction coefficients of treated samples are relatively stable (between 0.25 and 0.27). On the one hand, the oxide film on the sample surface is damaged during HCPEB process, then MgO film can not rapidly formed in the vacuum. On the other hand, the higher roughness on the surface will also lead to the increase in the friction coefficients. Compared to initial samples, the friction coefficients of Mg alloy AZ31 are obviously reduced after HCPEB bombardment. Additionally, the wear rate is reduced by a factor of 6.7 after 15 pulse treatment (as seen in Fig.3.3 (b)), so the wear resistance of Mg alloy AZ31 is increased significantly. It is indicated that there is a large potential in the application of Mg alloy AZ31 after HCPEB treatment.

Fig. 3.4 gives SEM morphologies of wear grooves on the surface of Mg alloy AZ31before and after HCPEB treatment. Compared to wear groove morphology on the surface of initial

(a) Friction coefficients                                    (b) Average friction rate
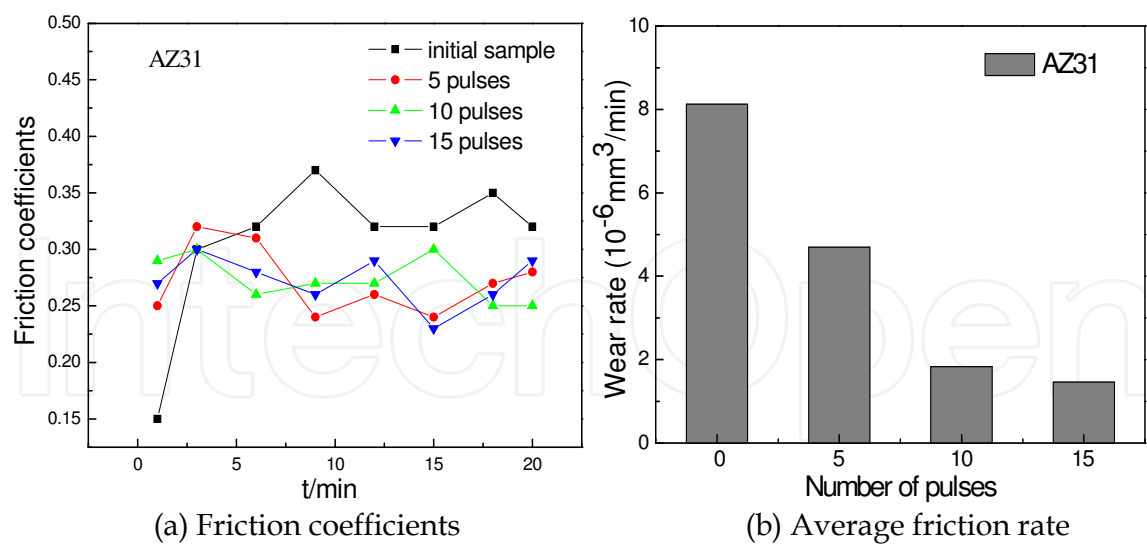
Fig. 3.3. Evolution of friction coefficients with friction time and change of average friction rate with the number of pulses for Mg alloy AZ31 before and after HCPEB treatment
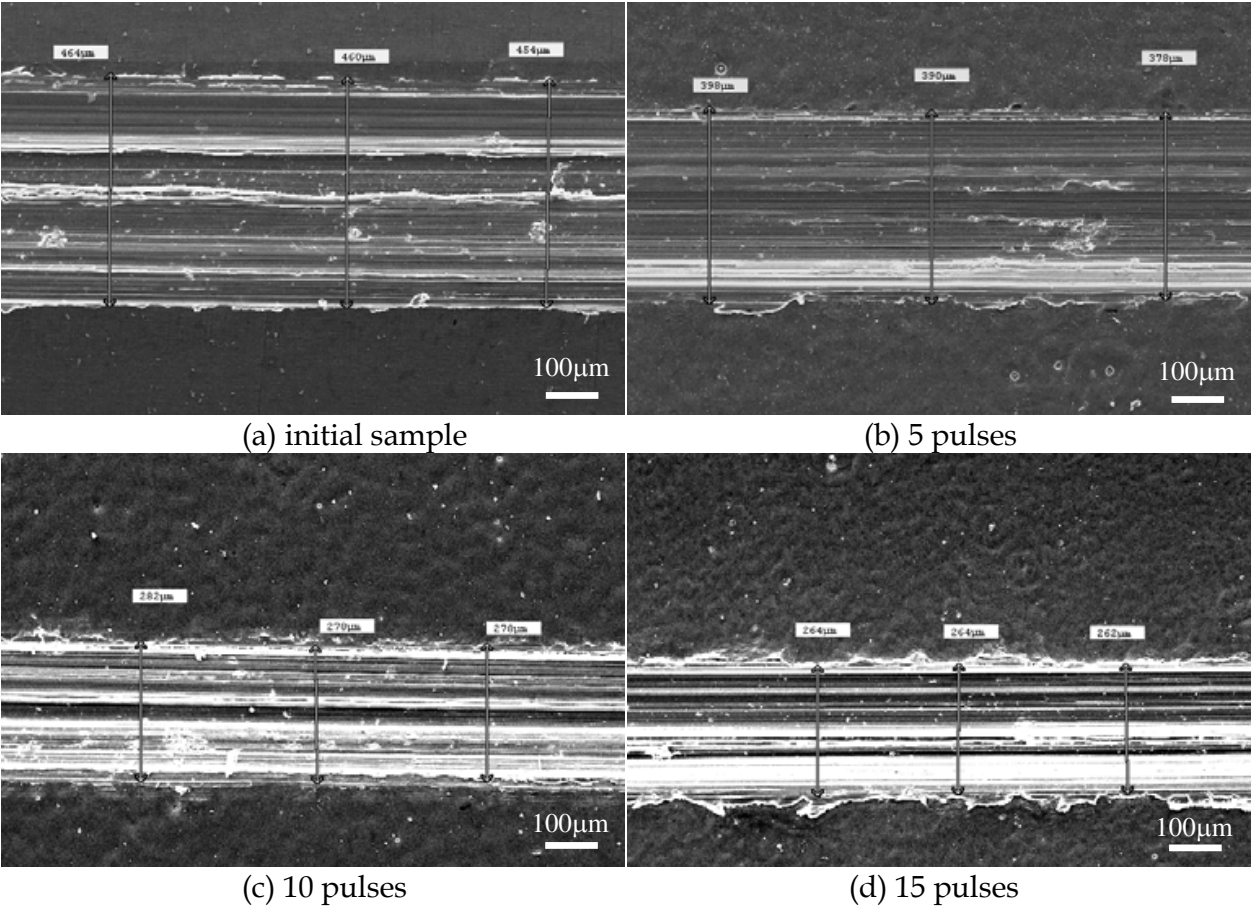


(a) initial sample                                                    (b) 5 pulses

(c) 10 pulses                                                        (d) 15 pulses

Fig. 3.4. SEM morphologies of wear grooves for Mg alloy AZ31 before and after HCPEB treatment with energy density of ~3J/cm²

sample, the width of wear grooves on the surface of Mg alloy AZ31 is decreased obviously after HCPEB treatment, which is reduced from 460μm of initial sample to 280μm of 10-pulse

treated sample. The wear form is the typical abrasive wear for Mg alloy AZ31. The hardness of matrix is far smaller than that of WC grinding ball, so the cutting form is focused on the wear surface and the groove morphology is formed. After HCPEB treatment, the residual compressive stress is left on the surface, leading to the increase in hardness of HCPEB-treated Mg alloy. As a result, the wear rate and wear volume are reduced, and the width of wear grooves is also decreased. Meanwhile, the main composition of wear debris is the oxides of Mg and Al through EDS analysis of SEM. It is caused by oxidization resulting from the fact that the wear test is performed in the atmosphere, and a lot of heat is accumulated on the sample surface during the severe friction process.

### 3.1.4 Corrosion resistance of Mg alloy AZ31

With focus on the problem of poor corrosion resistance of AZ31 Mg alloy in practical application (contact with atmosphere or sea water), this paper applies HCPEB to perform surface treatment in order to analyze the chemical composition of the surface remelted layer and discuss the change in corrosion resistance of Mg alloy AZ31 surface in 5%NaCl solution.

**3.1.4.1 Surface composition analysis of Mg alloy AZ31 before and after HCPEB surface treatment**

The chemical composition of alloy surface plays an important role in corrosion process. The changes of Mg, Zn and Al elements are analyzed by SEM. It is found that the variation of Zn is very small after HCPEB treatment. The changes of Mg and Al are mainly given in Fig. 3.5. It can be seen that the content of Mg on the surface is reduced after HCPEB treatment and reaches maximum reduction after 5 pulse treatment, which is due to Mg evaporation in the molten state. As the number of pulse increases to 10 pulses, the melted layer is thickened. The Mg contained underneath new melting liquid will spread or evaporate to the upper layer, so the Mg content on the surface of Mg alloy AZ31 will rise again. With further increase in pulse number, the Mg at the surface layer loses balance as well as the Mg inside the equipment, and the Mg at the surface layer evaporates, so the content of Mg is reduced again. But, the change of Al content is on the contrary to that of Mg. The increased Al content at the surface layer will be undoubtedly favorable to the formation of compact oxide film and the enhancement of corrosion resistance on the alloy surface. Therefore, in order to acquire the surface that contains high content of Al, it is crucial to choose proper pulse number and energy density.
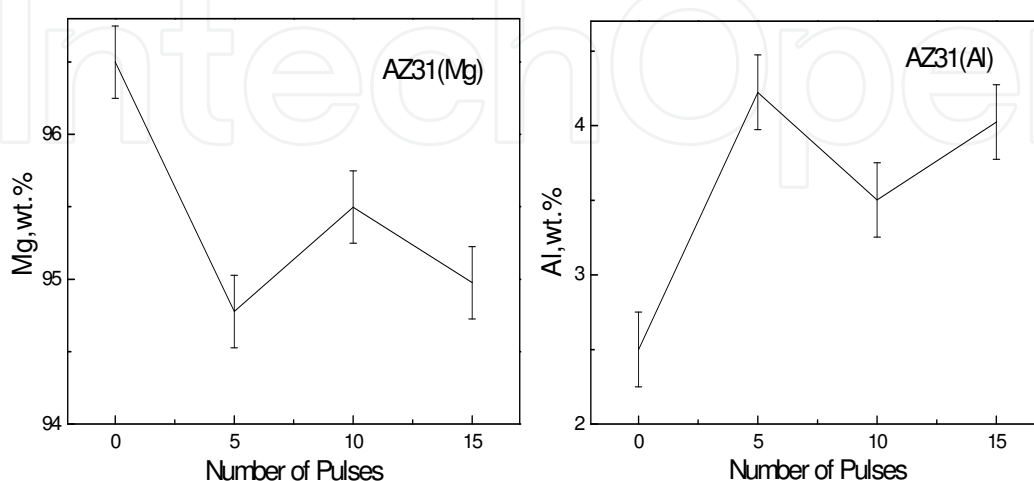


Fig. 3.5. Content of Mg and Al on the surface of Mg alloy AZ31 after HCPEB irradiation

### 3.1.4.2 Electrochemistry testing for Mg alloy AZ31

Fig. 3.6 shows the potentiodynamic polarization curves of Mg alloy AZ31 before and after HCPEB treatment. From the measuring result, we can see that the Ecorr of modified sample is moved to -1360mV. Through Tafel straight line fitting of cathode and anode, it is discovered that the corrosion current is reduced but the polarization resistance is increased. The reason is that HCPEB treatment leads to rich Al on the AZ31 Mg alloy surface and the formation of compact oxide film. Compared to the initial sample, the corrosion resistance of HCPEB-treated sample is increased. It can be also discovered that the overpotential (the difference between applied potential and Ecorr) reaches about 300mV, namely breakthrough occurs. For one thing, the surface protective film is comparatively thin. For another thing, the applied etching solution is 5% NaCl, in which chloride ion has strong penetrability. Hence the protective film is punctured rapidly. It also illustrates that HCPEB treatment can not be solely applied as the final process of the sample treatment, but it should be applied practically together with other processes.
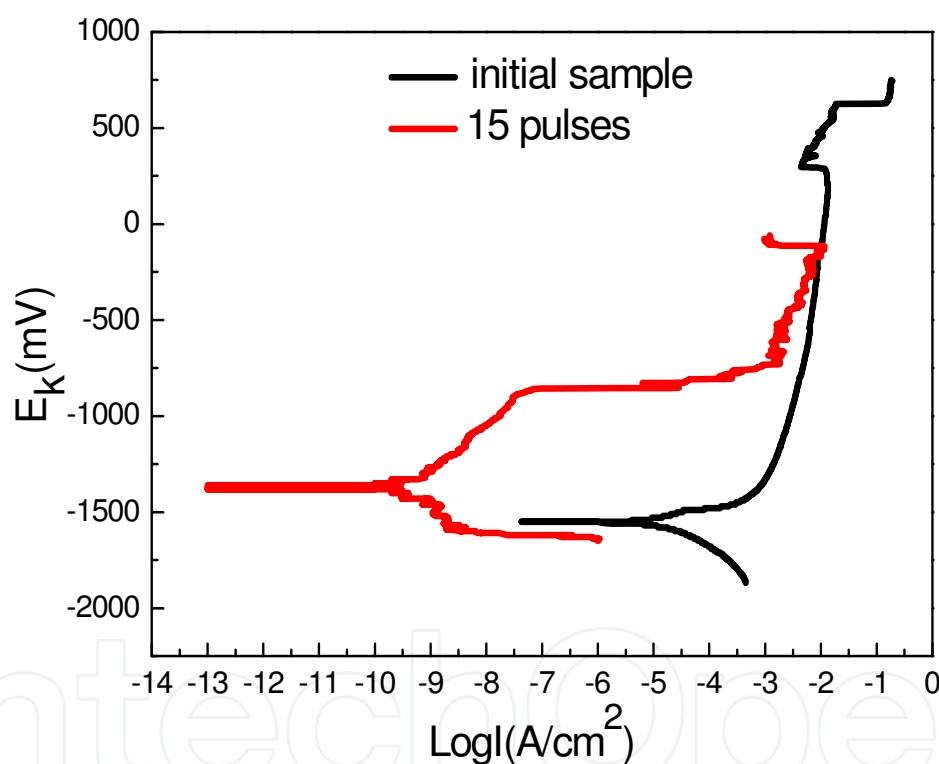


Fig. 3.6. Potentiodynamic polarization curves of Mg alloy AZ31 before and after HCPEB treatment (15 pulses)

### Analysis of corrosion mechanism

The corrosion of Mg alloy AZ31 is mainly divided into two stages: 1) the initial stage is controlled by galvanic corrosion; 2) the expansion stage is controlled by pitting.
The initial stage of corrosion:
In the neutral environment, a layer of protective $Mg(OH)_2$ thin film is formed on the surfaces of pure Mg and Mg alloy at the initial stage of corrosion, as shown in the following equation.

$$Mg + 2H_2O \rightarrow Mg(OH)_2 + H_2 \qquad (1)$$

Although Mg (OH) $_2$ has better protectiveness in the atmospheric environment, it alters [30] easily with the changes of electrochemistry and environmental conditions. The oxide grows initially from the crystal boundaries and extends into crystal grains. However, as for Mg alloy, the potential of crystal boundaries is higher than that of crystal grains, so the crystal boundaries form a galvanic couple with the crystal grains. The corrosion starts from the crystal boundaries and extends into crystal grains. Because the proportion of anode and cathode is larger and larger, the corrosion speed is accelerated with further corrosion. The rapid cooling （~$10^8$K/s） induced by HCPEB makes crystal grain fine and reduces the proportion of anode and cathode. Therefore, the corrosion current of the modified sample is smaller than that of the initial sample. Meanwhile, the increase in the solid solubility of Al will also increase the integral polarization resistance of the material. The first stage is finished when the material surface is covered with a layer of compact and stable magnesium hydroxide film.

The expansion stage of corrosion:

$$Mg^{2+} + 2Cl^- \rightarrow MgCl_2 + 2e^- \tag{2}$$

In the environment where the chloride ion exists, a sort of soluble magnesium salt forms in the boundary of metal and solution, as shown in the equation (2). This soluble magnesium salt ruins the protective film of magnesium hydroxide, and then the exposed metal generates self-solvent reaction with electrolyte in the damaged film and the corrosion speed is accelerated thereupon. The partial attack causes the pitting formed on the alloy surface. Once the pitting starts, it will expand at a very fast speed. Thinking over from the angle of kinetics, the pitting formation rate of the treated sample is smaller than that of the initial sample. It should be contributed to stability and compactness of oxide film formed on the surface of modified sample. It is equivalent that the anode dissolution speed is slowed down, thus Icorr is reduced remarkably.

## 3.2 Surface modification of Mg alloy ZK60-1Y by HCPEB

As for surface modification of Mg alloy ZK60-1Y by HCPEB treatment, the experiment process and parameters are similar to those of Mg alloy AZ31, namely accelerating voltage 27kV, energy density 3J/cm$^2$.

### 3.2.1 Surface morphology

Fig. 3.7 refers to surface SEM morphologies of Mg alloy ZK60-1Y before and after HCPEB treatment. Before electron beam treatment, the original structure of Mg alloy ZK60-1Y is composed by eutectic structure and matrix α(Mg), and the eutectic structure shows discontinuous distribution (white contrast in the figure), as shown in the Fig. 3.7 (a). After HCPEB treatment, the crystal boundaries on the surface of Mg alloy ZK60-1Y become less obvious, and the composition tends to be uniform. It is because that the HCPEB bombardment results in melting of the alloy surface, and it is too late to be redistributed and solidified for the elements owing to subsequent rapid solidification. At the same time, the typical "crater" morphology is formed on the surface of Mg alloy (Fig. 3.7 (b)). It is due to the ZK60-1Y Mg alloy surface is under the action of pulsed beam current, the subsurface is melted first and liquid is erupted outwards from inside, which is similar to the volcanic eruption. It is one reason for the formation of "crater" morphology [31]. With increasing pulse number, more energy is absorbed by the surface of Mg alloy, as a result, the "crater" quantity is reduced and the surface becomes much smoother, as shown in the Fig. 3.7 (c-d).
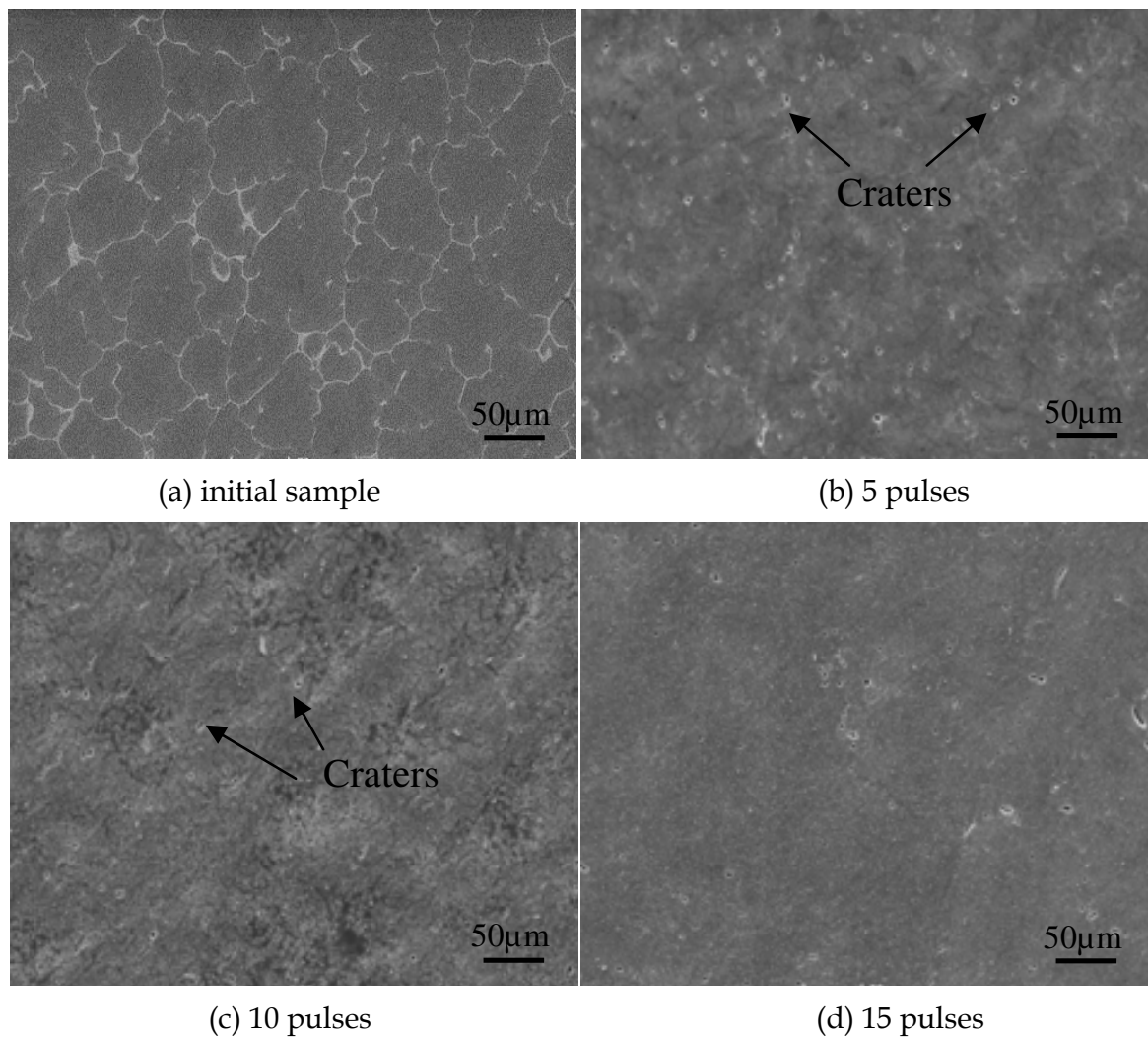
(a) initial sample                                    (b) 5 pulses

(c) 10 pulses                                          (d) 15 pulses

Fig. 3.7. Surface SEM morphologies of Mg alloy ZK60-1Y before and after HCPEB treatment



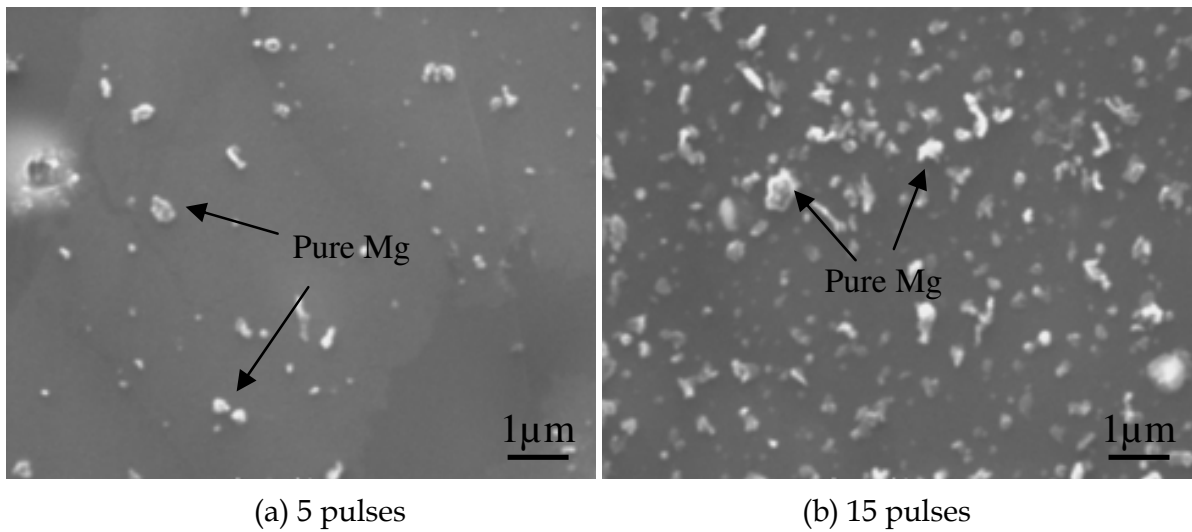(a) 5 pulses                                          (b) 15 pulses

Fig. 3.8. Pure Mg particles on the surface of Mg alloy ZK60-1Y after HCPEB treatment with accelerating voltage of 27kV

Fig. 3.8 shows pure Mg particles on the surface of Mg alloy ZK60-1Y after HCPEB treatment. From the figure, it can be seen that the pure Mg particles (the result of EDS analysis) are distributed on the surface of Mg alloy after HCPEB treatment and more pure Mg particles emerge on the alloy surface after 15 pulse treatment. The reason can be explained as follows: Mg belongs to the low melting point metal and its vapor pressure is also very low compared with Zr and Y elements. Under HCPEB bombardment, the temperature of matrix Mg rises swiftly due to the momentary energy deposition, resulting in melting of Mg at the surface layer. As the surface temperature reaches the boiling point, the vaporization goes ahead within a certain range at the surface layer and a lot of droplets sputter out. Because the target material surface parallels to the direction of gravity, the spilled droplets will not return to the surface under the action of gravity but will be charged with negative electricity under the action of electron beam current. As the target is the anode, the droplets with negative electricity will slow down and be drawn back to anode under the action of electric field force. Consequently, the droplets fall on the entire surface at certain speed. After solidification, we can see the pure Mg particles as shown in the Fig. 3.8.

### 3.2.2 Analysis of sectional microstructure
Fig. 3.9 refers to cross sectional SEM image of Mg alloy ZK60-1Y after HCPEB treatment. From the figure, it can be observed that remelted layer with thickness of ~12μm is formed on the surface layer. Compared to the matrix, the remelted layer is more compact and the crystal boundary become less obvious. It can mainly be explained as follows: the second phase existing in crystal boundaries melts and diffuses due to the rapid melting process induced by HCPEB treatment, while the crystal boundaries disappear in the melting liquid. When the electron beam bombardment terminates, the rapid solidification occurs immediately on the surface owing to good thermal conductivity of the metal material. Under the action of high solidification rate (~$10^8$K/s), great temperature gradient is generated on the surface of the material and non-equilibrium freezing occurs in the melting
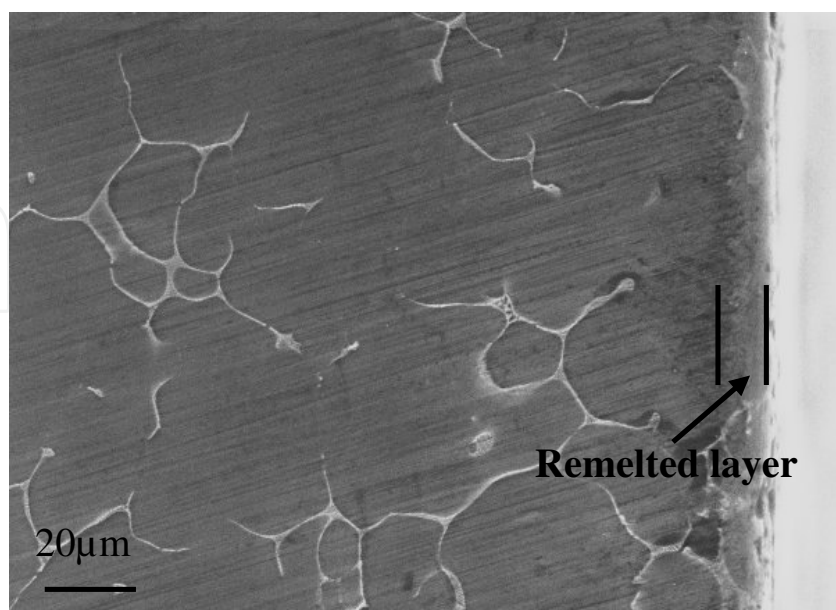


Fig. 3.9. Cross sectional SEM image of Mg alloy ZK60-1Y after HCPEB treatment after HCPEB treatment

layer. For the solidification time is too short, the actual temperature of the liquid at the frontier of solid liquid interface is lower than the liquidus temperature, so there is no way to provide continuous driving force for the growth of crystal grains. The nucleation rate of crystal is greater than the growth rate, so the crystal grains in the surface layer are refined and the inter-grain boundaries of the refined crystal grains become indistinct. In addition, the segregation phenomenon of alloying elements existing in grain boundaries is improved, and Zn and Zr better dissolve into the Mg matrix and form supersaturated solid solution. As a result, the element is uniformly distributed on the modified surface of Mg alloy ZK60-1Y.

### 3.2.3 Friction and wear property of Mg alloy ZK60-1Y before and after HCPEB treatment

Fig. 3.10 indicates the evolution of friction coefficients with the number of friction turns for Mg alloy ZK60-1Y before and after HCPEB treatment. From the figure, it can be seen that the friction coefficients of initial sample maintain around 0.28 at the initial friction stage. However, the friction coefficients of the sample are relatively high at the initial friction stage after 5 pulse treatment, around 0.35. It mainly because the sample surface is not even and the pure Mg particles are distributed on the modified surface, so the surface roughness is increased and the friction coefficients become higher. On the other hand, there is a layer of oxide film on the surface of the initial sample, and the surface roughness is smaller compared to that of the HCPEB-treated sample. Therefore, the friction coefficients of the initial sample are lower at the initial friction stage. With the increase in the number of friction turns, the friction coefficients of the initial sample present rising trend. Upon 1200 cycle friction, the friction coefficients maintain between 0.34 and 0.38. It is because that the oxide layer on the surface is worn away after a period of friction, therefore the matrix gradually touches stainless counterpart discs and shows high friction coefficients.
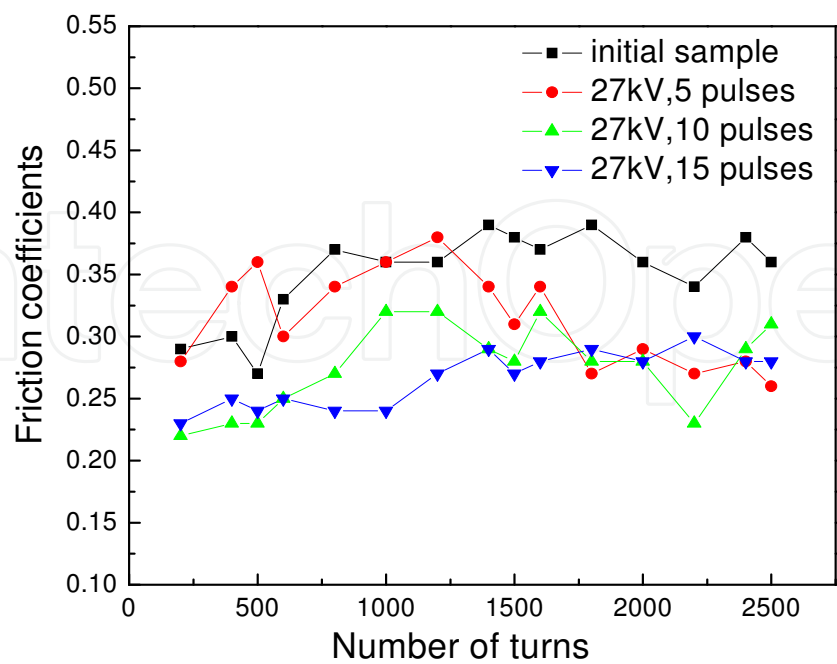


Fig. 3.10. Evolution of friction coefficients with the number of friction turns for Mg alloy ZK60-1Y before and after HCPEB treatment

After 1400 cycle friction, the friction coefficients of the sample treated by HCPEB are lower than that of the initial sample, showing better wear resistance. The reason can be summarized as:1) the grain structure in the remelted layer after HCPEB treatment is refined, namely fine-grain strengthening effect; 2)the enrichment phenomenon of alloying elements is improved, and the chemical composition is distributed evenly and the mechanical property is further enhanced on the ZK60-1Y Mg alloy surface. With the progressing of wear test (after 1800 cycle friction), the friction coefficients of HCPEB treated sample are much lower. It is because the surface at the remelted layer has been worn away basically. Then the remelted layer in this layer has better wear resistance. In the whole friction test, the friction coefficients of the alloy don't fluctuate drastically and maintain between 0.23 and 0.30 after 15 pulse treatment under the accelerating voltage of 27kV. With the increase of pulse number, the times of rapid solidification occurred on the treated sample surface is increased accordingly, thus the alloying elements are distributed evenly and the mechanical property of the alloy surface is more stable. To sum up, compared to the initial sample, the surface of Mg alloy ZK60-1Y has better wear resistance after HCPEB treatment.
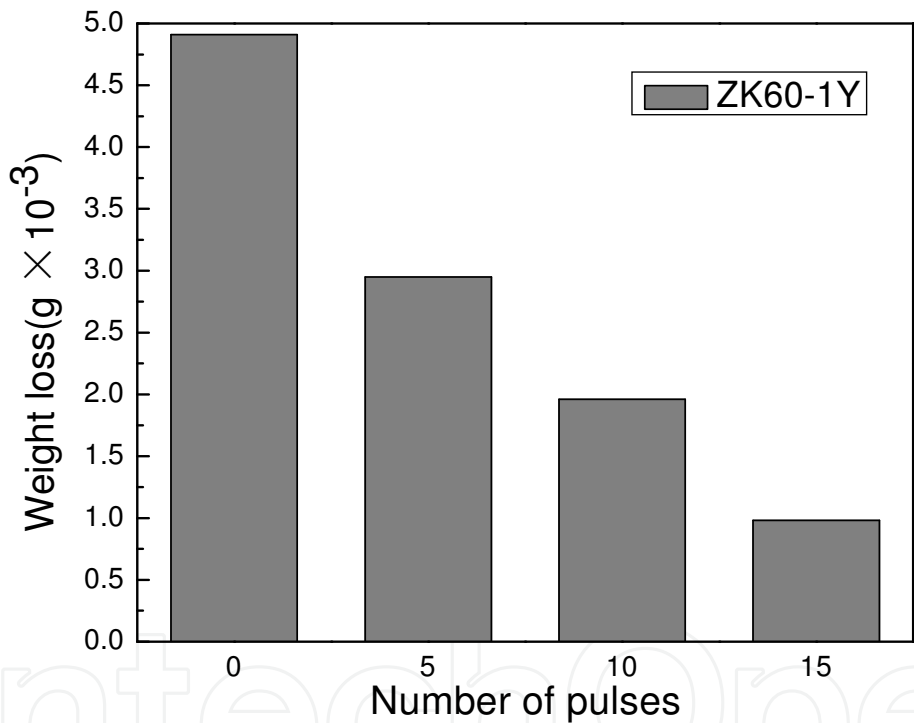


Fig. 3.11. Evolution of weight loss with the number of pulses for Mg alloy ZK60-1Y before and after HCPEB treatment

Fig. 3.11 refers to the evolution of weight loss with the number of pulses for Mg alloy before and after HCPEB treatment. From the figure, it can be seen that the weight loss of the sample is reduced from $4.91 \times 10^{-3}$g of initial sample to $0.98 \times 10^{-3}$g after 15 pulse treatment. It indicates that the wear resistance of the sample by HCPEB treatment is greatly improved under same friction condition. The weight loss of the sample by 5, 10 and 15 pulse treatments is reduced by 39.9%, 60.1%, 80% respectively compared to that of the initial sample. That means the wear resistance of the sample is the best after 15 pulse treatment under the accelerating voltage of 27kV and the relative wear resistance is improved by a factor of 5. It can be attributed to the changes in the microstructure of ZK60-1Y Mg alloy

surface after HCPEB treatment, namely composition homogenization (segregation reduction), grain refinement and the formation of supersaturated solid solution.

## 4. Conclusions

For the first time, the HCPEB technology is utilized to treat the surface of Mg alloys AZ31 and ZK60-1Y in the paper and perform the research into the changes in microstructure of Mg alloys before and after HCPEB treatment and the effect on the friction and wear property and corrosion resistance. The main conclusions are listed as below:

### 1) Mg alloy AZ31

After HCPEB irradiation of Mg alloy AZ31, wavy and "crater" morphologies and twins emerge on the modified surface. According to XRD analysis, it indicates that the diffraction peaks of Mg obviously move towards high-angle direction due to stresses existing in the surface layer induced by rapid solidification during HCPEB process.

After HCPEB treatment, the friction coefficients of Mg alloy AZ31 are reduced and the wear resistance is greatly improved. The wear resistance of the 15-pulsed sample is enhanced by about a factor of 6. Besides, the wear form is the typical abrasive wear. Meanwhile, the result of polarization curve test in 5%NaCl indicates that the corrosion resistance of the sample after HCPEB treatment is enhanced because the content of Al on the alloy surface is increased, and a layer of compact oxide film is formed on the surface. As a result, the polarization resistance is increased and the corrosion current is reduced.

### 2) Mg alloy ZK60-1Y

During the HCPEB treatment, the rapid melting and solidification process is completed on the surface of Mg alloy ZK60-1Y, and the grain boundaries on the surface become less obvious. The chemical composition tends to uniform distribution and some pure Mg particles are distributed on the alloy surface. According to the analysis of cross sectional structure, it indicates that a remelted layer with the thickness of ~12µm is formed on the surface of Mg alloy ZK60-1Y, which possesses much compact and refined structure compared to the matrix.

According to friction and wear test, the wear resistance of Mg alloy ZK60-1Y surface is obviously enhanced after HCPEB treatment and the friction coefficients and weight loss are reduced compared to that of the original sample. The wear resistance of Mg alloy ZK60-1Y by 15 pulse treatment is the best and the relative wear resistance is increased by a factor of 5.

## 5. Acknowledgements

## 6. References

[1] Liu X.B., Shan D.Y., Song Y.W. & Han E.H. (2010). Effects of heat treatment on corrosion behaviors of Mg-3Zn magnesium alloy, *Transactions of Nonferrous Metals Society of China* Vol.20 (No.7): 1345-1350.

[2] Feliu S. J., Pardo A., Merino M. C., Coy A. E., Viejo F. & Arrabal R. (2009). Correlation between the surface chemistry and the atmospheric corrosion of AZ31, AZ80 and AZ91D magnesium alloys, *Applied Surface Science* Vol.255 (No.7): 4102-4108.

[3] Candan S., Unal M., Koc E., Turen Y. & Candan E. (2011). Effects of titanium addition on mechanical and corrosion behaviours of AZ91 magnesium alloy, *Journal of Alloys and Compounds* Vol.509 (No.5): 1958-1963.

[4] Potzies C. & Kainer K.U. (2004). Fatigue of magnesium alloys, *Advanced Engineering Materials* Vol.6 (No.5): 281-289.

[5] Bin Sajuri Z., Umehara T., Miyashita Y. & Mutoh Y. (2004). Fatigue-Life Prediction of Magnesium Alloys for Structural Applications, *Advanced Engineering Materials* Vol.5 (No.12): 910-916.

[6] Song G.L. & Atrens A. (1999). Corrosion mechanisms of magnesium alloys, *Advanced Engineering Materials* Vol.1 (No.1): 11-33.

[7] Wu K., Wang Y.Q. & Zheng M.Y. (2007). Effects of microarc oxidation surface treatment on the mechanical properties of Mg alloy and Mg matrix composites, *Materials Science and Engineering A* Vol.447 (No.1-2): 227-232.

[8] Chen C.J., Wang M.C., Wang D.S., Jin R. & Liu Y.M. (2007). Microstructure and corrosion behavior of Mg-Nd coatings on AZ31 magnesium alloy produced by high-energy micro-arc alloying process, *Journal of Alloys and Compounds* Vol.438 (No.1-2): 321-326.

[9] Jiang B.L., Zhang S.F., Wu G.J. & Lei T.Q. (2002). Microflaw and phases constitution of ceramic coating formed by micro-arc oxidation on magnesium alloys and their influence on corrosion-resistance, *The Chinese Juranl Nonferrous metals* Vol.12 (No.3): 454-457.

[10] Apelfeld A. V., Bespalova O. V., Borisov A. M., Dunkin O. N., Goryaga N. G., Kulikauskas V. S., Romanovsky E. A., Semenov S. V. & Souminov I. V. (2000). Application of the particle backscattering methods for the study of new oxide protective coatings at the surface of Al and Mg alloys, *Nuclear Instruments and Methods in Physics Research B* Vol.161-163: 553-557.

[11] Wang Y.M., Wang F.H., Xu M.J., Zhao B., Guo L.X. & Ouyang J.H.(2009). Microstructure and corrosion behavior of coated AZ91 alloy by microarc oxidation for biomedical application, *Applied Surface Science* Vol.255 (No.22): 9124-9131.

[12] Abbas G., Liu Z.& Skeldon P. (2005). Corrosion behaviour of laser-melted magnesium alloys, *Applied Surface Science* Vol.247 (No.1-4): 347-353 .

[13] Dutta Majumdar J., Galun R., Mordike B. L. & Manna I. (2003). Effect of laser surface melting on corrosion and wear resistance of a commercial magnesium alloy, *Materials Science and EngineeringA* Vol.361 (No.1-2): 119-129 .

[14] Samant Anoop N., Du Baoshuai, Paital Sameer R., Kumar S. & Dahotre Narendra B.(2009). Pulsed laser surface treatment of magnesium alloy: Correlation between thermal model and experimental observations, *Journal of Materials Processing Technology* Vol.209 (No.11): 5060-5067.

[15] Mondal A.K., Kumar S., Blawert C. & Dahotre Narendra B. (2008). Effect of laser surface treatment on corrosion and wear resistance of ACM720 Mg alloy, *Surface and Coatings Technology* Vol.202 (No.14): 3187-3198.

[16] Dutta Majumdar J. & Manna I.(2010). Mechanical properties of a laser-surface-alloyed magnesium-based alloy (AZ91) with nickel, *Scripta Materialia* Vol.62 (No.8): 579-581.

[17] Bohne Y., Seeger D.M., Blawert C., Dietzel W., Mändl S. & Rauschenbach B. (2006). Influence of ion energy on properties of Mg alloy thin films formed by ion beam sputter deposition, *Surface and Coatings Technology* Vol.200 (No.22-23): 6527-6532.

[18] Li P., Lei M.K., Zhu X.P., Han X.G., Liu C. & Xin J.P. (2010). Wear mechanism of AZ31 magnesium alloy irradiated by high-intensity pulsed ion beam, *Surface and Coatings Technology* Vol.204 (No.14): 2152-2158.

[19] Yang J.X., Cui F.Z., Lee In-Seop, Jiao Y.P., Yin Q.S. & Zhang Y. (2008). Ion-beam assisted deposited C-N coating on magnesium alloys, *Surface and Coatings Technology* Vol.202 (No.22-23): 5737-5741.

[20] Zou J.X., Grosdidier T., Zhang K.M. & Dong C. (2009). Cross-sectional analysis of the graded microstructure in an AISI D2-steel treated with low energy high-current pulsed electron beam, *Applied Surface Science* Vol.255 (No.9): 4758-4764.

[21] Hao S.Z, Zhang X.D., Mei X.X., Grosdidier T. & Dong C.(2008). Surface treatment of DZ4 directionally solidified nickel-based superalloy by high current pulsed electron beam, *Materials Letters* Vol.62 (No.3): 414-417.

[22] Dong C., Wu A., Hao S., Zou J., Liu Z., Zhong P., Zhang A., Xu T., Chen J., Xu J., Liu Q. & Zhou Z.(2003). Surface treatment by high current pulsed electron beam, *Surface and Coatings Technology* Vol.163-164: 620-624.

[23] Surzhikov A.P., Frangulyan T.S., Ghyngazov S.A. & Koval N.N. (2009). Structural-phase transformations in near-surface layers of alumina-zirconium ceramics induced by low-energy high-current electron beams, *Nuclear Instruments and Methods in Physics Research B* Vol.267 (No.7): 1072-1076.

[24] An J., Shen X.X., Lu Y. & Liu Y.B.(2006). Microstructure and tribological properties of Al-Pb alloy modified by high current pulsed electron beam, *Wear* Vol.261 (No.2): 208-215.

[25] Hao Y., Gao B., Tu G.F., Li S.W., Hao S.Z. & Dong C.(2011). Surface modification of Al-20Si alloy by high current pulsed electron, *Applied Surface Science* Vol.257 (No.9): 3913-3919.

[26] Zhang K. M., Zou J. X., Grosdidier T., Gey N., Weber S., Yang D. Z. & Dong C.(2007). Mechanisms of structural evolutions associated with the high current pulsed electron beam treatment of a NiTi shape memory alloy, *Journal of Vacuum Science and Technology A* Vol.25 (No.1): 28-36.

[27] Proskurovsky D.I., Rotshtein V. P., Ozur G. E., Markov A. B., Nazarov D. S., Shulov V. A., Ivanov Yu. F. & Buchheit R. G. (1998). Pulsed electron-beam technology for surface modification of metallic materials, *Journal of Vacuum Science and Technology A* Vol.16 (No.4): 2480-2488.

[28] Guan Q.F., Zhang Q.Y., Dong C. & Zou D.T. (2005). Deformation twining in single-crystal aluminum induced by high-current pulsed electron beam, *Journal of Mterials Science* Vol.40 (No.18): 5049-5052.

[29] Gao B., Hao S.Z., Zou J. X., Wu W. Y, Tu G.F. & Dong C. (2007). Effect of high current pulsed electron beam treatment on surface microstructure and wear and corrosion resistance of an AZ91HP magnesium alloy, *Surface and Coatings Technology* Vol.201 (No. 14): 6297-6303.

[30] Mizutani Y., Kim S. J., Ichino R. & Okido M. (2003). Anodizing of Mg alloys in alkaline solutions, *Surface and Coatings Technology* Vol.169-170: 143-146.

[31] Qin Y., Dong C., Wang X.G., Hao S.Z., Wu A.M., Zou J.X. & Liu Y. (2003). Temperature profile and crater formation induced in high current pulsed electron beam processing, *Vacuum Science and Technology A* Vol.21 (No.6): 1934-1938.
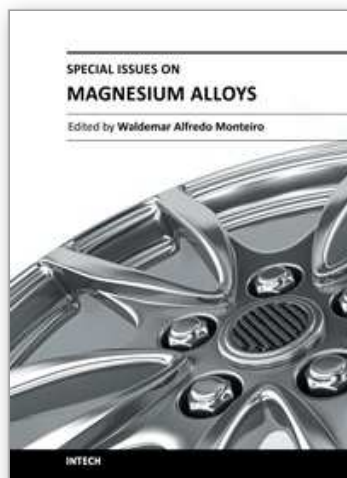
**Special Issues on Magnesium Alloys**

Edited by Dr. Waldemar Monteiro

Magnesium is the lightest of all the metals and the sixth most abundant on Earth. Magnesium is ductile and the most machinable of all the metals. Magnesium alloy developments have traditionally been driven by requirements for lightweight materials to operate under increasingly demanding conditions (magnesium alloy castings, wrought products, powder metallurgy components, office equipment, nuclear applications, flares, sacrificial anodes for the protection of other metals, flash photography and tools). The biggest potential market for magnesium alloys is in the automotive industry. In recent years new magnesium alloys have demonstrated a superior corrosion resistance for aerospace and specialty applications. Considering the information above, special issues on magnesium alloys are exposed in this book: casting technology; surface modification of some special Mg alloys; protective carbon coatings on magnesium alloys; fatigue cracking behaviors of cast magnesium alloys and also, magnesium alloys biocompatibility as degradable implant materials.

**How to reference**

In order to correctly reference this scholarly work, feel free to copy and paste the following:

Gao Bo, Hao Yi, Zhang Wenfeng and Tu Ganfeng (2011). Surface Modification of Mg Alloys AZ31 and ZK60-1Y by High Current Pulsed Electron Beam, Special Issues on Magnesium Alloys, Dr. Waldemar Monteiro (Ed.), ISBN: 978-953-307-391-0, InTech, Available from: http://www.intechopen.com/books/special-issues-on-magnesium-alloys/surface-modification-of-mg-alloys-az31-and-zk60-1y-by-high-current-pulsed-electron-beam

# INTECH
open science | open minds